Characterization of GOES-16 ABI Detector-Level Uniformity from Post-Launch North South Scan Collections of Several Earth Targets

Jason Casey*[a], Francis Padula[a], Monica Cook[a], Brent Bartlett[a], Aaron Pearlman[a], Dave Pogorzala[b], & Changyong Cao[c]
[a]GeoThinkTank LLC, Washington, DC USA 20009; [b]Integrity Applications Incorporated, Chantilly, VA USA 20151; [c]NOAA/NESDIS/STAR College Park, MD USA 20740

ABSTRACT

The GOES-16 Advanced Baseline Imager (ABI) is the first of four of NOAA's new generation of Earth imagers. The ABI uses large focal plane arrays (100s to 1000s of detectors per channel), which is a significant increase in the number of detectors per channel compared to the heritage GOES O-P imagers (2 to 8 detectors per channel). Due to the increase in number of detectors there is an increased risk of imaging striping in the L1b & L2+ products. To support post-launch striping risk mitigation strategies, customized ABI special scans (ABI North South Scans - NSS) were developed and implemented in the post-launch checkout validation plan. ABI NSS collections navigate each detector of a given channel over the same Earth target enabling the characterization of detector-level performance evaluation. These scans were used to collect data over several Earth targets to understand detector-to-detector uniformity as function of a broad set of targets. This effort will focus on the data analysis, from a limited set of NSS data (ABI Ch. 1), to demonstrate the fundamental methodology and ability to conduct post-launch detector-level performance characterization and advanced relative calibrations using such data. These collections and results provide critical insight in the development of striping risk mitigation strategies needed in the GOES-R era to ensure L1b data quality to the GOES user community.

Keywords: GOES-R, ABI, North-South Scans, Calibration/Validation, Relative Calibration, Image Striping

1. INTRODUCTION

The GOES-16 Advanced Baseline Imager (ABI) is the first of four of NOAA's new generation of Earth imagers providing significant spatial, spectral, and temporal observational enhancements, as well as enhanced capabilities for operational sensor calibration and image navigation and registration (INR) compared to the heritage GOES imagers [1-3]. ABI provides imagery of the Earth's weather, oceans, and environment in 16 spectral channels (six Reflective Solar Bands (RSB) and 10 Thermal Emissive Bands (TEB)). The new system leverages Focal Plane Arrays (FPA) that collect large swaths of the Earth (~500 km with each west-east scan) with 100s to 1000s of detectors per channel. The number of ABI detectors per channel is a significant increase in compared to the heritage GOES O-P imagers (2 to 8 detectors per channel). This is critically important since large FPAs can exhibit variances in at sensor radiance due to various effects such as pixel to pixel differences in detector response, optical effects, and electronic noise that can introduce artifacts in the imagery [4]. As a result, the increase in number of detectors, increases the risk of image striping (detector-to-detector non-uniformities) in the ABI series of L1b & L2+ products. The large FPAs also introduce new challenges in post-launch calibration/validation (Cal/Val) of GOES imagers due to the fact that an ABI swath coverage is much larger than a single uniform Earth Cal/Val target. This highlights a major post-launch validation challenge in the GOES-R ABI era that requires new validation strategies to be developed to ensure the post-launch performance of all detectors of the ABI [5]. To address these challenges customized ABI special scans (ABI North South Scans - NSS) were developed and implemented to provide advanced Cal/Val post-launch capabilities.

In this paper preliminary analysis and development of a post-launch detector-level performance characterization capability that leverages customized collections is demonstrated. An introduction of ABI NSS will be discussed in the next section, followed by a discussion of NSS data sampling, data processing, and application leveraging a limited set of data. This preliminary analysis will be used to demonstrate the utility of the detector-level uniformity characterization, relative gain generation, and the potential to advance post-launch Cal/Val capabilities for the GOES-R series of ABI instruments. For this initial demonstration only the reflective solar bands will be used, but the approach

Earth Observing Systems XXIII, edited by James J. Butler, Xiaoxiong (Jack) Xiong, Xingfa Gu, Proc. of SPIE Vol. 10764, 107640D · © 2018 SPIE · CCC code: 0277-786X/18/$18 · doi: 10.1117/12.2323673

is applicable in the thermal emissive bands as well. Note the objective of this effort is to demonstrate the methodology of using ABI NSS as a post-launch performance Cal/Val capability.

1.1 ABI North South Scan Overview

The ABI instrument has two independent scanning mirrors (a North-South scan mirror & an East-West scan mirror) that facilitate a flexible set of collection capabilities [1]. Nominal ABI Earth collection is conducted by sweeping the detectors west-to-east for a single swatch, and incrementally the north-to-south scan mirror for each successive swath [Figure 1 (Full Disk & Regional)].The nominal scan data is processed from raw digital counts (L0 data) to calibrated and navigated samples (L1β) and then navigated to a fixed grid by resampling individual detector samples (L1b). ABI NSS collections navigate each detector of a given channel over the same Earth target by holding the east-west scan mirror fixed and moving the north-south scan mirror. In practice, both east-west and north-south scan mirrors should be moved to ensure a north-south footprint is collected. It requires 16 unique NSS swaths (one per channel) to observe the same target with each channel. This enables the characterization of detector-level performance. Raw L0 ABI NSS data is processed to L1β to maintain the capability for analyzing detector response differences.

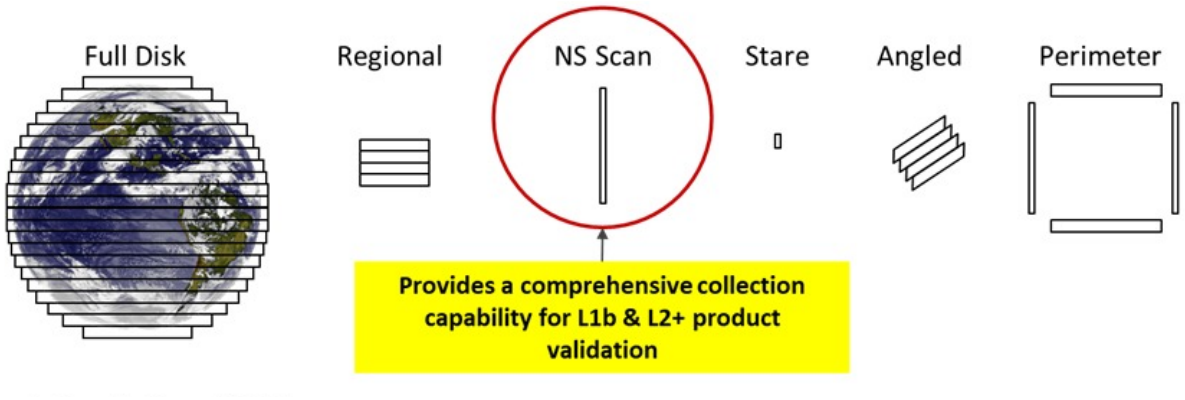

Figure 1. Illustrates ABI scan flexibility highlighting the North-South (NS) Scan. Note nominal collection is represented by Full Disk and Regional scanning. This graphic is adopted courtesy of Harris Corporation.

ABI NSS are essentially equivalent to the mature Low Earth Orbit (LEO) pushbroom sensing community's side-slither technique that is conducted by a 90 degree yaw maneuver of the spacecraft to enable all detectors to collect over the same effective target area providing an ideal method of on-orbit relative calibration (detector-to-detector non-uniformity characterization) [4-8]. This effort will illustrate how lessons learned in the LEO large FPA community can be applied to the GOES-R ABI era data stream.

2. METHODOLOGY & APPROACH

Two ABI NSS collections, one of the Sonoran Desert at the United States and Mexico border on August 19, 2017 and one of the Uyuni Salt Flats in Bolivia on August 29, 2017, were used for this effort. Both collections provide imagery of a uniform desert region as Earth vicarious validation targets [9]; the collection of the Sonoran Desert also provides NSS data over a uniform ocean region (due to the proximity of the ocean to the Sonoran target site). This results in three target regions of interest for this initial study. Each collection generates four or five NSS per channel for the target of interest. This analysis will consider a single NSS collected for ABI Ch. 1 over each target. Table 1 summarizes the data discussed in this effort.

Table 1. Summary of NSS collections used in this paper.

Target	Date and Time	Data Analyzed
Sonoran Desert Region	August 19, 2017	GOES-16 ABI NSS Ch. 1
Bolivian Salt Flat	August 29, 2017	GOES-16 ABI NSS Ch. 1

2.1 NSS Data Sampling

The extent of a single NSS scan is shown in Figure 2; a NSS is approximately 2000 km in length to ensure sufficient overlap over each target. Because of the orientation of the FPA, not all detectors image the same area on the ground for a complete scan. The portion of the NSS imaged by all detectors is referred to as the overlap region. In Figure 2 (a), the start and stop locations of the first (southernmost detector on the FPA) and last (northernmost detector on the FPA) detectors is shown along with the overlap region. An illustration of the raw data from an entire NSS is shown in Figure 2 (b). Each row in the image represents the magnitude of the radiance data from a single detector. Each detector collects the same number of samples; however, because of the collection methodology as shown in Figure 2, the first sample for each detector does not correspond to the same location on the Earth. Manipulation of this data for processing will be discussed in the following section.

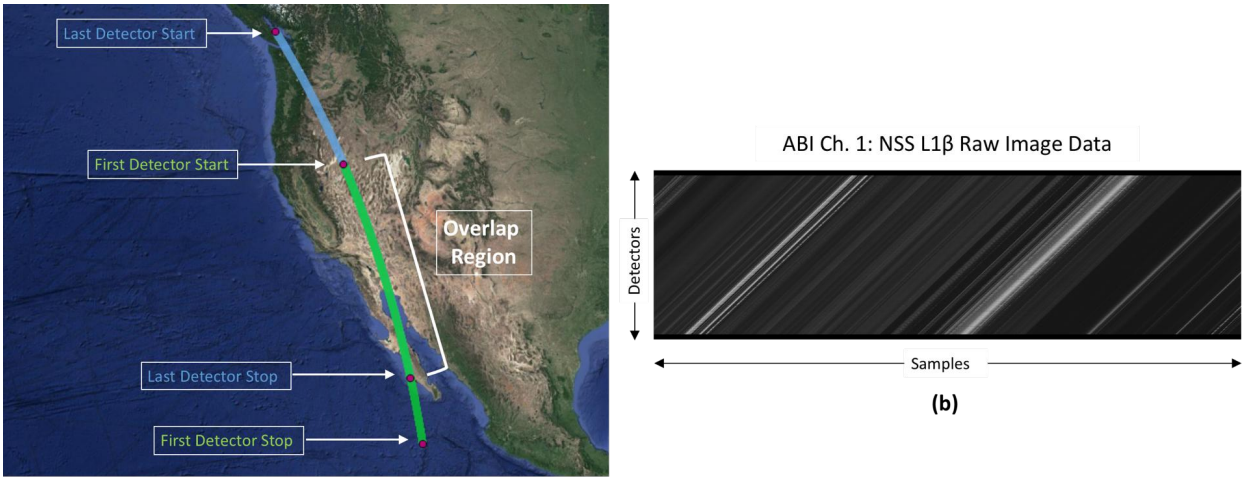

Figure 2. An illustration of the extent of a single NSS over the Sonoran Desert target projected onto the Earth, as well as the start and stop locations of the first and last detectors, which determine the overlap region (a). An image of the raw data from a NSS over the Sonora Desert target is shown in (b).

2.2 Data Processing

One of the main takeaways that this paper is demonstrating is the robustness of approach using geospatial analytical techniques to analyze the data. This section will illustrate and discuss the fundamentals of how the data is prepared for superpixel generation and analysis of gain derivation.

First, the overlap region [Figure 3 (a)] must be sub-selected from the raw data. Only locations on the ground that were imaged by all detectors will be considered; adjacent pixels in the adjusted image overlap the same region on the Earth. Note that there is no image processing done in this step; pixel indices are selected based on their geospatial location. The tools developed, along with the NSS image data processed to level L1β, allow for navigating earth locations on a per-pixel basis without performing image warping or orthorectification which could introduce artifacts in the data impacting analysis.

This data is then optimized for processing. Each column in Figure 3 (b) portrays the response of each detector over the same location on the Earth, enabling detector-level performance evaluation. In Figure 3, the green lines highlight a single location on the ground in both the original overlap region [Figure 3 (a)] and data optimized for processing [Figure 3 (b)]. This illustrates how the optimized structure of the image data facilitates detector-level analysis from the NSS data. Wide homogenous vertical stripes are uniform regions within the scene. Narrow horizontal streaks are mostly due to detector-to-detector non-uniformity. Techniques for using the NSS data to generate relative gains that can eliminate horizontal streaks in the imagery will be discussed below. If the regions imaged are uniform, and the detector response is uniform, the horizontal streaks would not be present in the imagery.

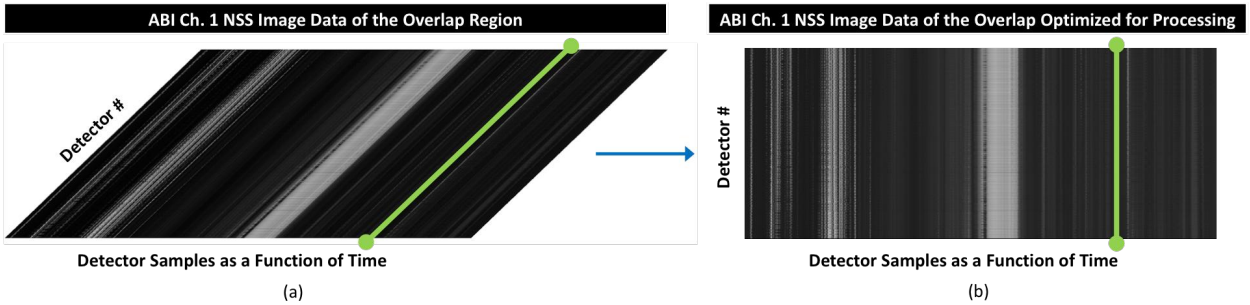

Figure 3. Illustrates ABI NSS image data (Bolivia - August 29, 2017) of the overlap region (a) and the ABI NSS image data optimized for processing (b). The green lines shown in (a) & (b) highlight a single location on the ground to illustrate the structure of the image data to facilitate detector-level analysis of the NSS data.

2.3 Identification of Superpixels

Once the data has been manipulated and optimized for processing, a uniform subset region is selected for further investigation. This region is referred to here as a superpixel, and contains at a minimum one sample of every detector in a given ABI channel. The superpixel is constructed by seeking to maximize the north-south extent of the data region selected (i.e largest uniform area possible in the north-south direction) to encompass multiple samples of each detector, in a given channel, to reduce noise and any Earth surface inhomogeneity effects. Analysis is conducted without the need for any reprojection or imaging processing because the L1β data is already navigated (i.e. latitude & longitude locations of each pixel).

Radiance values from an extended area (within the overlap region) both including and beyond the target area were plotted. This region is illustrated by the purple box in Figure 4 (a); note that this is a large area that contains the desert target location and also includes the ocean to the south and populated regions to the north. For each detector, the radiance values sampled within the purple box are plotted in Figure 4 (b). The northernmost sample in the purple box corresponds to sample 0 in the plot such that samples from north to south in Figure 4 (a) are plotted left to right in Figure 4 (b).

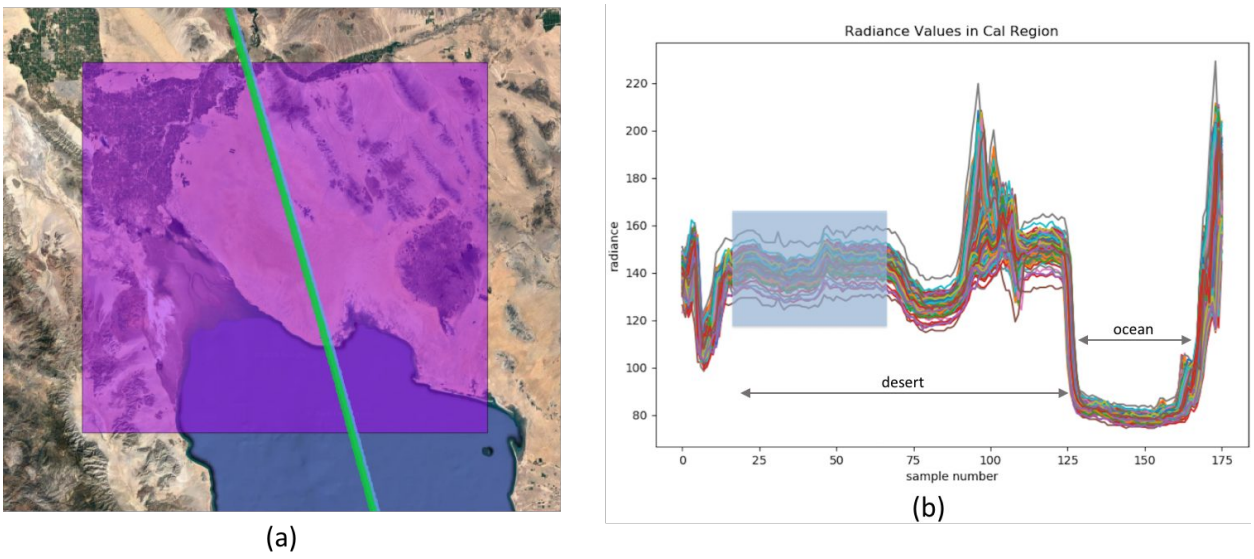

Figure 4. (a) A large extended region, including and beyond the target area, used to evaluate the uniformity of detector samples when identifying a superpixel region. (b) ABI Ch 1 radiance values for an extended region. A low sample number represents a northern point and a large sample number a southern point, such that the box north-south is represented by a line left to right in the plot above. Different lines represent different detectors.

Figure 4 (b) illustrates the radiance as a function of sample number for all detectors from ABI Ch. 1 from the overlap region. Uniform regions can be identified through visual inspection of the data as regions that are flat. Note the desert has small regions of uniformity, interrupted by regions of greater variability caused by Earth surface changes, likely

in terrain and surface properties. As the surface transitions from desert to open ocean, the radiance values are shown to significantly decrease.

A superpixel region(s) can be generated from this data [Figure 4 (b)] through several approaches, such as geospatial query, statistical techniques, or a combination of the two. A simple geospatial query approach was used to generate the superpixel of interest [Figure 5]. Figure 5 illustrates the footprints of all detector samples encompassing a single superpixel for ABI Ch. 1 in the Sonoran Desert. Note the slight differences in detector footprint locations are due to the band dependent column numbers of each ABI FPA - assumed negligible (i.e. uniform region) for this analysis.

Figure 5. An ABI NSS superpixel of ABI Ch. 1 detector samples footprints (all detectors) defined in the Sonoran Desert on August 19, 2017.

2.4 Generation of Relative Gains

ABI is an absolutely calibrated radiometer and the details of the absolute calibration are beyond the scope of this paper, but can be found in [1]. Calibration of the ABI data is performed in the generation of the L1β product. The goal of the relative calibration is to mitigate detector-to-detector non-uniformity or image striping by generating a set of relative gains that scale the values of each detector relative to all other detectors within the channel - "flat fielding". The relative gain (g_{rel}) defined here accounts for the residual detector-to-detector calibration differences not captured by the ABI calibration equation. The relative gain ($g_{rel,\,ch,\,i}$) is calculated for each channel on a per detector basis as:

$$g_{rel,ch,i} = \frac{\overline{L_i}}{\overline{L_{ch}}} \qquad \text{Eq. 1}$$

where $\overline{L_i}$ is the average radiance value of all samples within the superpixel for detector i and $\overline{L_{ch}}$ is the average radiance value for all samples within the superpixel for all detectors in channel ch. The relative gains can be obtained from many different approaches using different targets, temporal data sets, and/or FPA specific characteristics (detector dependent vs column dependent). For this study, Eq. 1 was used to generate all results using detector-level processing only. Comparison of gains from each site [Table 1] are used to characterize the detector-level response as a function of target type from this limited data set.

2.5 Application and Assessment of Relative Gains

The derived relative gains [Section 2.3] enable the assessment of non-uniformity corrections in the ABI nominal scan imagery. To investigate, the derived relative gains from each target site were applied to a nominal swath ABI L1β imagery by simply multiplying the ABI L1βradiance data by Eq 1, resulting in imagery using the the relative gains. Through comparison of the original ABI L1βswath to the updated ABI L1β swath (relative gain applied) an assessment of image quality was performed. Image quality was characterized both qualitatively and quantitatively through visual inspection and use of Eq. 2, respectively. A streaking metric was used to compute uniformity

performance over a scene. The streaking metric referenced in [7] was used here, and is shown in Equation 2, where $\overline{Q}_i$ is a detector of interest and $\overline{Q}_{i-1}$ and $\overline{Q}_{i+1}$ are adjacent detectors.

$$S_i = \frac{\left|\overline{Q}_i - \frac{1}{2}\left(\overline{Q}_{i-1} + \overline{Q}_{i+1}\right)\right|}{\overline{Q}_i} \qquad \text{Eq. 2}$$

This effort will focus on the data analysis and results from these tests in support of detector-level performance characterization and advanced calibration methodologies.

3. RESULTS

Using the methodology described above [Section 2 and illustrated in Figures 4 & 5] superpixels were selected for each target location (shown between the vertical lines of Figure 6) from the ABI Ch. 1 NSS data collections [Table 1]. Analysis of Figure 6 shows that each superpixel region is unique in both magnitude and variability with the ocean target (darker) demonstrating lower detector-to-detector variability [Figure 6 (a)] and desert targets (brighter) showing higher variability [Figure 6 (b & c)]. The relative gains calculated from each superpixel region are shown in Figure 7. The ocean and Sonora target regions generated relative gains that are more similar to one another compared to the brighter target region over Bolivia. The relative gains from the Bolivian Desert track the results using the ocean and Sonora targets, but are generally higher in magnitude compared to the gains generated from the darker target regions. Note that the variability in sensor response is significantly larger over the Bolivian target in Figure 6 (c) compared to the Sonoran target in Figure 6 (b). The larger relative gains over the brighter target regions, along with the observed larger variability in detector responses might indicate an uncharacterized nonlinear detector response over a large dynamic range from the given state of the calibration at the time of the collection.

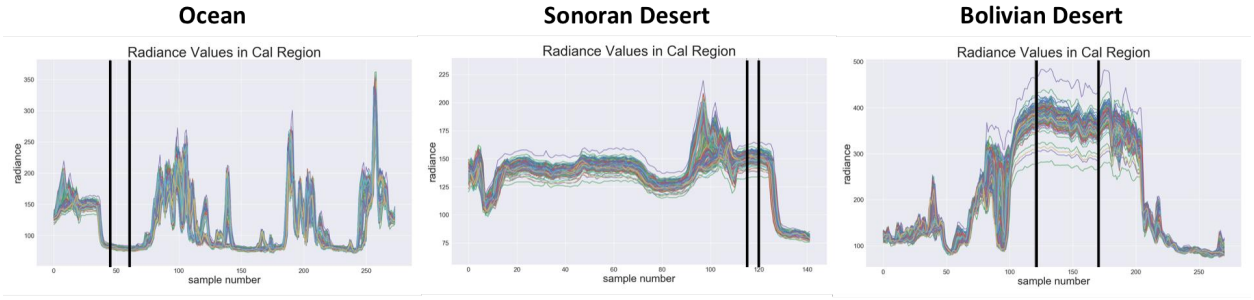

Figure 6. Illustrates ABI Ch. 1 NSS radiance data from a subset of the overlap region (i.e. all detectors) as a function of time, with the identified superpixel regions shown (between the black lines) for each target region.

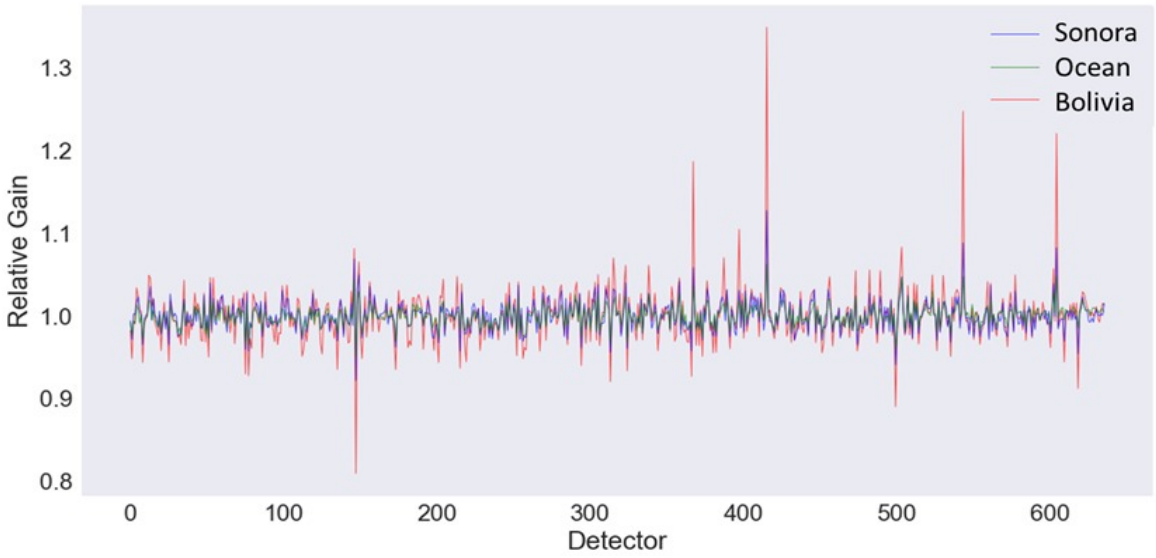

Figure 7. Relative gains derived from each target region.

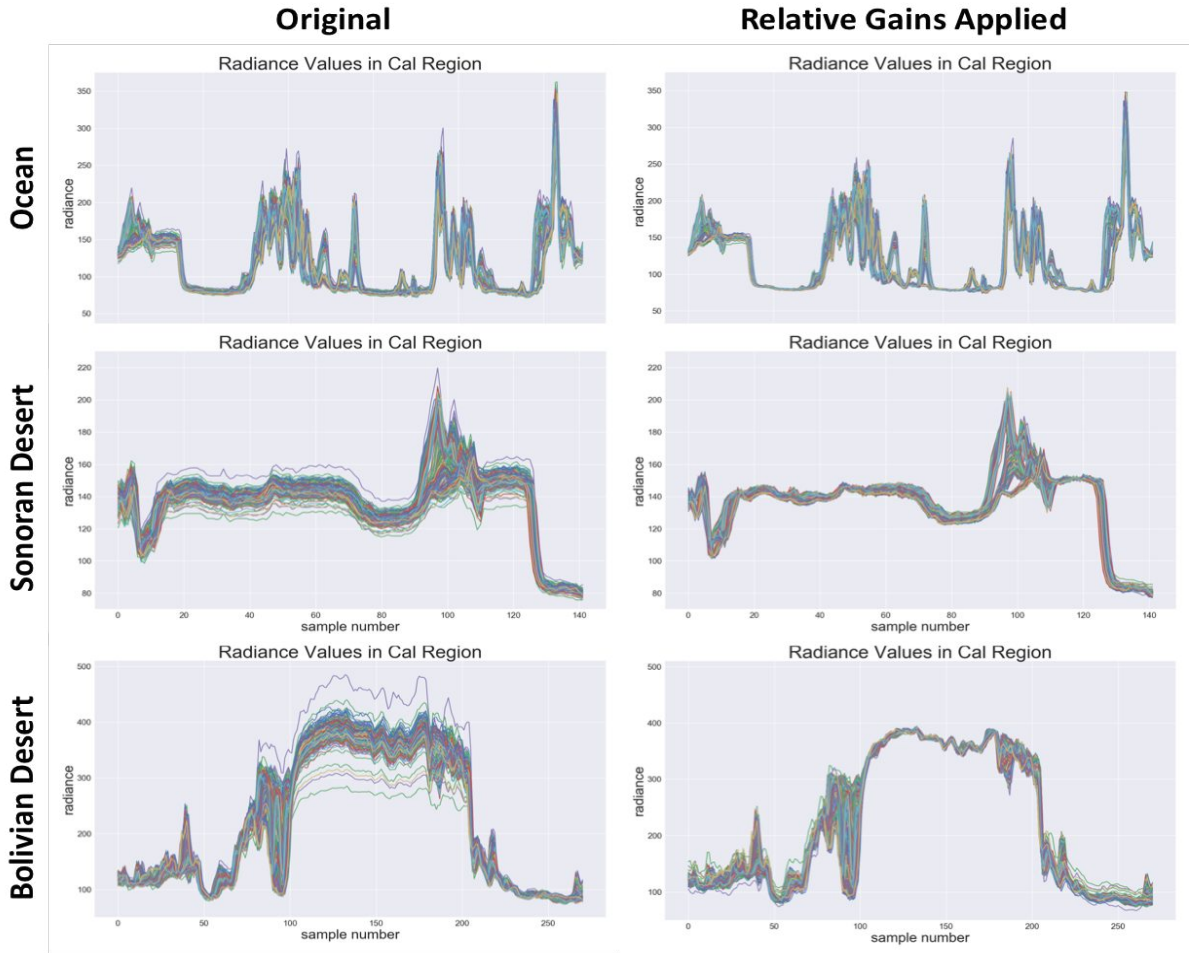

Figure 8. Illustrates ABI Ch. 1 NSS radiance data with the derived relative gains applied (right); for comparison the original radiance data is shown (left).

The relative gains were applied to each corresponding NSS region [Figure 8]. Detector-to-detector variability appears to decrease in each case, especially near the radiance values in the selected superpixel region. It can be noted, however, that some detector-to-detector variability increases in the lower portion of the dynamic range over the Bolivian Desert after relative gains are applied, as shown in Figure 8. This could, again, indicate a nonlinear response over a large dynamic range.

Relative gains from each target location were applied to a meso image swath containing a large, bright cloud, as shown in Figure 9. The results show, visually, that uniformity over this image is improved by applying the relative gains computed over each target region, especially as the brightness of the target region increases. Figure 9 (d) shows a significant visual improvement to the imagery compared to the original image in Figure 9 (a). This makes sense physically because the Bolivian Desert radiance levels are most similar to those of the cloud region resulting in more uniform detector-to-detector performance. This suggest that some non-linearity behavior exists given the differences in performance as a function of scene brightness. The detector spectral response uniformity across the FPA may also impact the scene-dependency of the flat field results [10-12]. These qualitative results demonstrate how the NSS data can be used to assess detector-to-detector uniformity, and potentially be used to generate operational relative gains to improve the visual image quality of the ABI data.

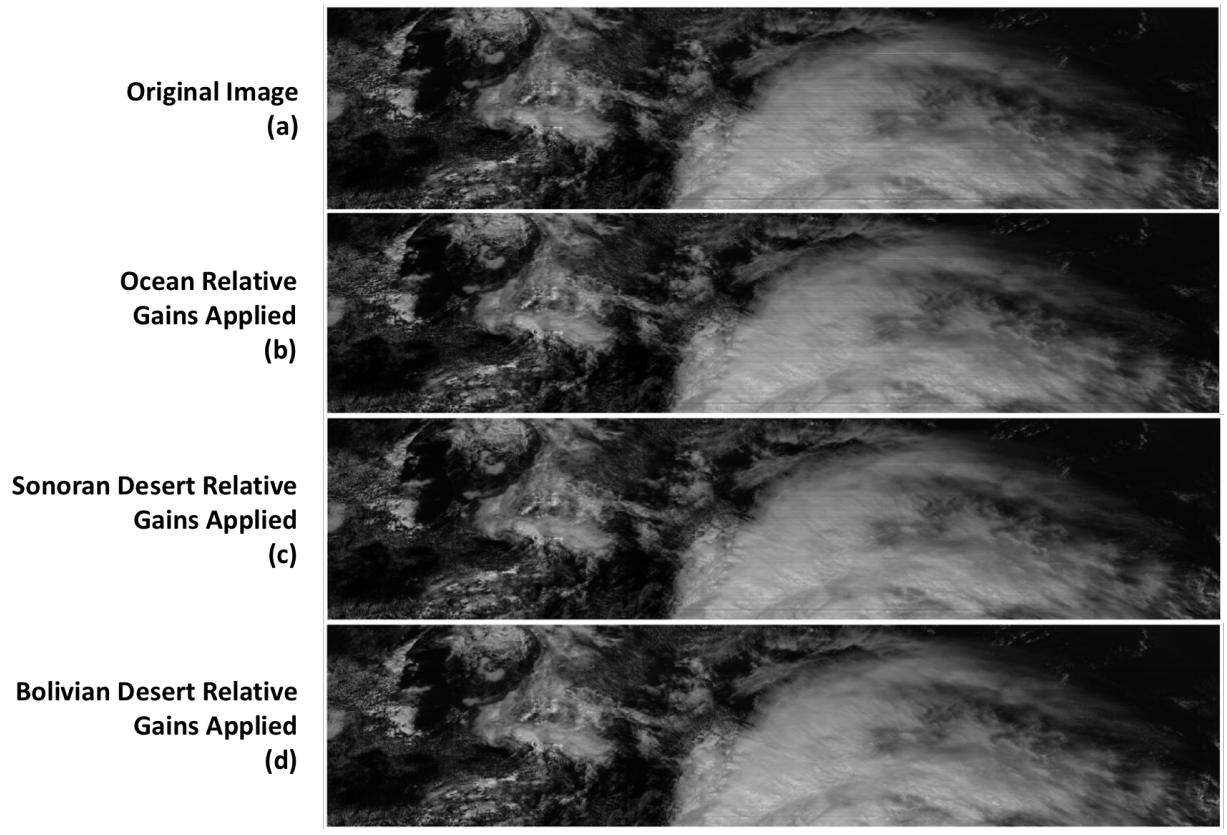

Figure 9. Relative gains applied to imagery. Original image (a), relative gains derived from ocean target applied to image (b), relative gains derived from Sonoran Desert applied to image (c), relative gains derived from Bolivian Desert applied to image (d).

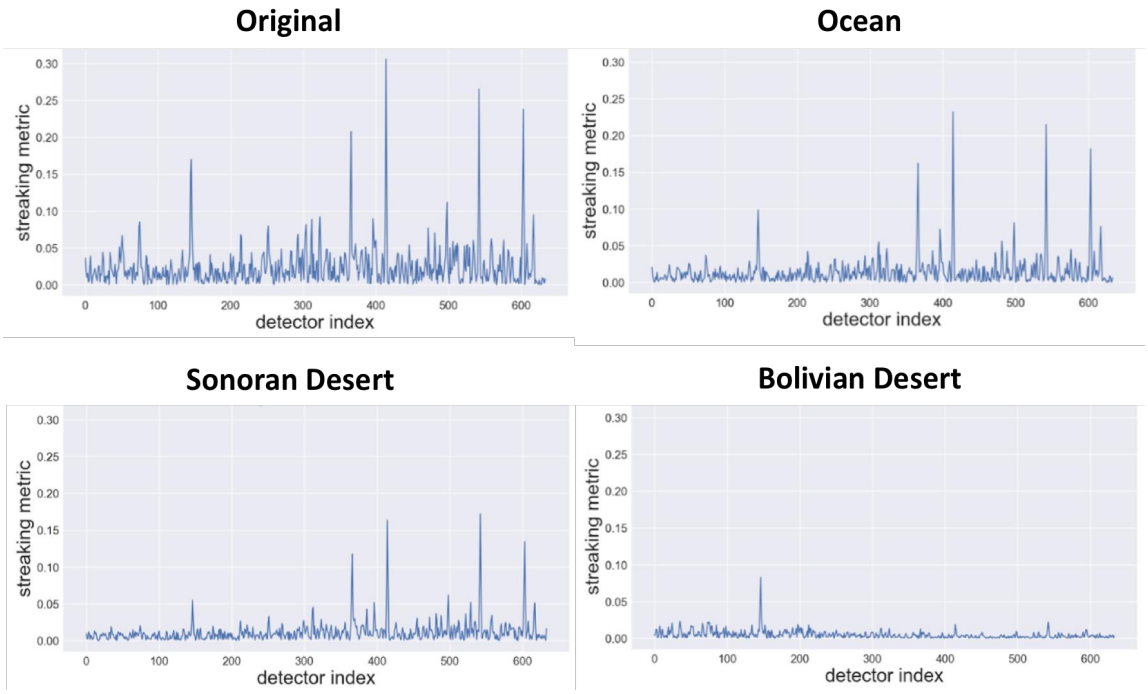

Figure 10. Streaking metric applied to each image shown in Figure 9.

Quantitative analysis of performance was also conducted by calculating the streaking metric [Eq. 2] for each image swath shown in Figure 9; the streaking metric values for the original imagery and imagery with relative gains applied for each target region is shown in Figure 10. Analysis of Figure 10 indicates that uniformity over this bright image is improved when relative gains are applied in all cases. The metric also indicates that uniformity improves as the target region used to generate the relative gains increases in brightness. This makes sense, as discussed above since the Bolivian Desert target is closest in brightness to the clouds in the image swath used in this study. The fact that the streaking metrics are significantly better using relative gains over the bright Bolivian Desert region is another indication of nonlinear detector response; this further illustrates that uniformity over a scene can be achieved using gains derived from a region with the same general brightness as that image the relative gains are being applied to. The relative calibration method (i.e. flat-fielding) is ideally suited for detectors that exhibit linear behavior, and is more challenging where non-linear behavior is found meaning more advanced methods may need to be developed.

4.0 SUMMARY

The ABI series of imagers provide critical new insights and advanced environmental observations of the Earth compared to heritage GOES imagers. To address the new validation challenges introduced by the ABI, customized ABI special scans were developed and implemented. In this initial demonstration study a new methodology was introduced that illustrated a fundamental approach of how to utilize ABI NSS data to enable customized and advanced post-launch detector-level calibration/validation capabilities to this class of imaging system. This initial study was limited in scope and future work will expand on this effort by applying this approach to all ABI bands and exploring the various ways to process the data to optimize performance. These collections and results provide critical insights in the development of striping risk mitigation strategies needed in the GOES-R ABI era to ensure L1b data quality to the GOES user community.

ACKNOWLEDGEMENTS

This work is funded by the GOES-R Program. The manuscript contents are solely the opinions of the authors and do not constitute a statement of policy, decision, or position on behalf of NOAA or the U.S. government.

REFERENCES

[1] Kalluri, S., Alcala, C., Carr, J., Griffith, P., Lebair, W., Lindsey, D., Race, R., Wu, X., Zierk, S., "From Photons to Pixels: Processing Data from the Advanced Baseline Imager," Remote Sens. 2018, 10, 177.

[2] Schmit, T. J., Paul Griffith, Mathew M. Gunshor, Jaime M. Daniels, Steven J. Goodman and William J. Lebair, "A Closer Look at the ABI on the GOES-R Series," Bull. Am. Meteor. Soc., doi: 10.1175/BAMS-D-15-00230.1, 2016.

[3] GOES-R website, "Advanced Baseline Imager," https://www.goes-r.gov/spacesegment/abi.html, July 2018.

[4] Henderson, B.G. and Krause, K.S., "Relative radiometric correction of QuickBird imagery using the side-slither technique on orbit", Proc. SPIE 5542, Earth Observing Systems IX, (26 October 2004); doi: 10.1117/12.559910; https://doi.org/10.1117/12.559910.

[5] Padula, F., Pearlman, A., Cao, C., Goodman, S., "Towards post-launch validation of GOES-R ABI SI traceability with high-altitude aircraft, small near surface UAS, and satellite reference measurements," Proc. SPIE 9972, Earth Observing Systems XXI, 99720V (19 September 2016); doi: 10.1117/12.2238181.

[6] Anderson, C., Naughton, D., Brunn, A., Thiele, M., "Radiometric correction of RapidEye imagery using the on-orbit side-slither method." Proc. SPIE 8180, Image and Signal Processing for Remote Sensing XVII, 818008 (27 October 2011); doi: 10.1117/12.898411.

[7] Pesta, F., Bhatta, S., Helder, D., Mishra, N., "Radiometric Non-Uniformity Characterization and Correction of Landsat 8 OLI Using Earth Imagery-Based Techniques." Remote Sens. 2015, 7, 430-446; doi:10.3390/rs70100430.

[8] Gerace, A., Schott, J., Gartley, M., and Montanaro, M., "An Analysis of the Side Slither On-Orbit Calibration Technique Using the DIRSIG Model", Remote Sens., 6, (2014).

[9] Committee on Earth Observation Satellites (CEOS): http://ceos.org/ourwork/workinggroups/wgcv/.

[10] Efremova, B., Pearlman, A.J., Padula, F., Wu, X., "Detector level ABI spectral response function: FM4 analysis and comparison for different ABI modules," Proc. SPIE 9972, Earth Observing Systems XXI, 99720S (19 September 2016).

[11] Pearlman, A.J., Padula, F., Cao, C., Wu, X., "The GOES-R Advanced Baseline Imager: detector spectral response effects on thermal emissive band calibration," Proc. SPIE 9639, Sensors, Systems, and Next-Generation Satellites XIX, 963917 (12 October 2015).

[12] Padula, F., Cao, C., "GOES-R ABI Detector-Level Spectral Response Function Performance Characterization, IGARSS. Oral Presentation. Milan Italy, (July 2015).